Improved superscaling description of electron and charged-current neutrino quasielastic scattering using effective mass dynamics

V. L. Martinez-Consentino,[1,2,*] P. R. Casale,[3,4,†] and J. E. Amaro[3,4,‡]

[1]*Departamento Sistemas Físicos Químicos y Naturales, Universidad Pablo de Olavide, Sevilla, E-41013, Spain*

[2]*Departmento de Ciencias Integradas, Universidad de Huelva, E-21071 Huelva, Spain*

[3]*Departamento de Física Atómica, Molecular y Nuclear Universidad de Granada, E-18071 Granada, Spain*

[4]*Instituto Carlos I de Física Teórica y Computacional, Universidad de Granada, E-18071 Granada, Spain*

(Received 5 June 2025; accepted 28 July 2025; published 21 August 2025)

We present an improved version of the Superscaling Analysis with Relativistic Effective Mass, denoted as SuSAM-v2. In the original SuSAM model, a universal scaling function was fitted to a selected set of quasielastic electron scattering (e, e') cross section data, using a phenomenological ansatz inspired by the relativistic mean field model of nuclear matter. In this work, we refine the procedure by first fitting a longitudinal scaling function directly to experimental longitudinal response data. Subsequently, a separate transverse scaling function is extracted from purely transverse data, after subtracting the longitudinal contribution already determined. We find that the resulting transverse scaling function must exhibit an explicit dependence on the momentum transfer q in order to reproduce all kinematics consistently. The resulting SuSAM-v2 model simultaneously describes inclusive quasielastic cross sections and both longitudinal and transverse response functions in electron scattering. The model is then applied to neutrino-nucleus scattering, showing an improved prediction compared to the previous SuSAM-v1 version, due to a more accurate treatment of the relative contributions of the longitudinal and transverse weak nuclear responses.

DOI: 10.1103/1njz-1m49

I. INTRODUCTION

Electron and neutrino scattering from nuclei play a central role in advancing our understanding of nuclear dynamics and in the interpretation of neutrino oscillation experiments [1,2]. In the case of electron scattering, precise measurements provide access to the charge and current distributions involved in nuclear transitions [3]. For neutrino interactions, a detailed knowledge of neutrino-nucleus cross sections is essential for reconstructing the incident neutrino energy in oscillation analyses [4,5]. However, modeling lepton-nucleus interactions is challenging due to the complexity of nuclear effects. Approaches such as the relativistic Fermi gas (RFG) provides a simple baseline description of the quasielastic (QE) cross section [6], but they lack important features such as medium modifications, finite-size effects, nuclear correlations, and final-state interactions. More refined nuclear models are therefore required to achieve an accurate and reliable description of the data.

A wealth of studies have been devoted to modeling the intricate nuclear dynamics underlying electron and neutrino scattering. Among these are relativistic distorted-wave impulse approximation models based on the nuclear shell structure [7–9], continuum random phase approximation approaches that include long-range correlations [10–12], and spectral function models that provide a detailed account of single-particle motion and nucleon-nucleon correlations [2,13]. Additional sophistication is introduced through the inclusion of meson-exchange currents (MEC) [14–16], short-range (SRC) and tensor correlations [17], and final-state interactions [18]. Moreover, *ab initio* methods such as Green's function Monte Carlo are increasingly able to describe light- and medium-mass nuclei with high precision [19–21]. While these approaches yield valuable insights, they are computationally demanding and often limited in scope when applied to the full range of kinematics or nuclear targets needed in neutrino oscillation experiments. Moreover, despite the level of sophistication

*Contact author: victormc@ugr.es
†Contact author: palomacasale@ugr.es
‡Contact author: amaro@ugr.es

achieved in these theoretical approaches, they often lead to different predictions for the cross section or response functions under comparable kinematic conditions, making it difficult to establish a unique and reliable description of the data.

In this context, simpler yet accurate frameworks that capture the dominant physics across many nuclei and kinematics remain essential. Models based on superscaling provide semiphenomenological parametrizations of the inclusive quasielastic cross section [22]. They typically assume a factorization between an average single-nucleon cross section and a function that encapsulates the effective number of nucleons that can be excited by transferring momentum q and energy ω [23,24]. This function, closely related to the integrated hole-spectral function, represents the distribution of available nucleons capable of undergoing a transition within the energy interval $[\omega, \omega + d\omega]$. By dividing out the known RFG dependence on q and k_F, and the single-nucleon dynamics, one arrives at a universal scaling function, $f(\psi)$, that ideally depends only on a single dimensionless variable ψ characterizing the kinematics of the one-body nuclear response [25].

In the original superscaling analysis (SuSA) approach, the phenomenological longitudinal scaling function $f_L(\psi)$ was extracted from selected quasielastic longitudinal response data [22,26]. It was then assumed that the transverse scaling function $f_T(\psi)$ could be approximated by the same function, $f_T(\psi) \approx f_L(\psi)$, in accordance with the idea of zeroth-kind scaling [27]. However, this assumption proved to be inconsistent with experimental data, where a transverse enhancement is significant [28–30]. In the updated SuSA-v2 framework, the transverse response was instead modeled using results from the relativistic mean field (RMF) approach, which better captured the observed behavior [31,32]. This improvement required introducing a mild but necessary q-dependence in the transverse scaling function, thereby explicitly breaking superscaling in that channel while preserving agreement with data.

In this work, we build upon the superscaling analysis with relativistic effective mass (SuSAM), a variant of SuSA designed to improve the description of quasielastic (e, e') data by incorporating nuclear dynamics inspired by the RMF theory of nuclear matter [33,34]. The motivation for using RMF-inspired dynamics lies in its long-standing success in describing the shape and magnitude of the quasielastic response [35,36]. Unlike the original SuSA approach, which is based on the RFG with a fixed nucleon mass and a phenomenological energy shift, SuSAM introduces a dynamical ingredient at the single-nucleon level through the use of a relativistic effective mass M^*, as derived from the Walecka model [37,38]. This approach embeds medium effects from the outset and preserves gauge invariance, which is not guaranteed in the traditional SuSA prescription. Another key difference is the fitting strategy: while SuSA derives the scaling function from selected longitudinal response data, SuSAM directly fits a phenomenological scaling function to selected quasielastic cross section data. This strategy allows for a global analysis of inclusive electron scattering data and has been successfully used to extract the effective mass M^* and Fermi momentum k_F for a wide range of nuclei across the periodic table [34]. The model has also demonstrated good predictive power for neutrino-nucleus cross sections, particularly after including contributions from two-particle–two-hole (2p2h) excitations computed consistently within the same RMF framework [39–41].

Despite the success of SuSAM in describing inclusive quasielastic cross sections, it falls short when it comes to reproducing the individual longitudinal and transverse nuclear responses. This limitation arises because the model was directly fitted to inclusive (e, e') cross section data, which effectively represent a weighted average of the longitudinal and transverse components. As a result, SuSAM does not provide sufficient control over each response separately, especially at low-momentum transfer. This issue becomes particularly relevant for neutrino-nucleus scattering, where the longitudinal and transverse responses enter the cross section in a different combination than in electron scattering, and where additional contributions from the axial current also play a role.

In this work, we propose an improved scaling analysis—SuSAM-v2—that aims to overcome this limitation. The model builds upon the SuSAM framework by preserving its key dynamical ingredient, the relativistic effective mass, while introducing a more constrained and controlled extraction of the scaling functions. Specifically, we fit the longitudinal scaling function to data on the separated longitudinal response and simultaneously to inclusive (e, e') cross sections. The transverse response is not fitted directly but emerges as a prediction of the model. Remarkably, this approach leads to a good description of all available data, including both separated response functions and inclusive cross sections, thus providing a more robust foundation for neutrino cross section predictions.

As in the case of SuSA-v2, this strategy entails introducing a transverse scaling function that exhibits an explicit dependence on the momentum transfer q. Nevertheless, this q-dependence can be captured through a simple analytical parametrization, which maintains the overall transparency and usability of the model. Superscaling-based models such as SuSAM$^*v2$ and SuSA-v2 rely on a phenomenological analysis aimed at reproducing experimental data with minimal theoretical assumptions. This approach enhances their utility in practical applications, such as neutrino event generators, but also highlights the importance of recognizing their intrinsic limitations, particularly concerning the microscopic nuclear dynamics that are not explicitly modeled.

The work is organized as follows: in Sec. II, we present a summary of the formalism for electron scattering, including the cross section structure, the RMF model for nuclear matter, and the superscaling approach incorporating an effective nucleon mass. In Sec. III, we outline the development of the SuSAM-v2 model, describing the modifications introduced to improve the separate description of the nuclear response functions. In Sec. IV, we compare the predictions of SuSAM-v2 with experimental data from both electron and CC neutrino scattering. Finally, Sec. V contains our conclusions.

II. FORMALISM

The starting point for the scaling analysis of the quasielastic response is traditionally the RFG model, which provides a simple framework including basic features of the momentum distribution of the nucleons with Fermi momentum k_F, and the one-body interaction with the lepton. In the SuSAM approach, this starting point is extended by incorporating RMF dynamics. The nucleons are now described as relativistic plane waves moving in the presence of a (constant) RMF that includes both scalar and vector components. The attractive scalar potential lowers the mass of the nucleons, giving rise to a relativistic effective mass $m_N^* = M^* m_N$, with $M^* < 1$, typically $M^* = 0.8$ for ^{12}C. The repulsive vector potential shifts the energy levels upward. As a result, the total energy of a nucleon in the medium is given by

$$E_{\mathrm{RMF}} = E + E_v,$$

where $E = \sqrt{(m_N^*)^2 + p^2}$ is the on-shell energy of a nucleon with momentum $\mathbf{p}$, and E_v is the vector potential energy. For ^{12}C, $E_v = 141$ MeV (see Ref. [42]).

The (e, e') cross section in plane-wave approximation can be written as a linear combination of longitudinal and transverse response functions

$$\frac{d\sigma}{d\Omega' d\epsilon'} = \sigma_{\mathrm{M}}(v_L R_L(q,\omega) + v_T R_T(q,\omega)). \tag{1}$$

Here, σ_M is the Mott cross section, q is the momentum transfer, ω the energy transfer, and the four-momentum transfer verifies $Q^2 = \omega^2 - q^2 < 0$. The kinematical factors are

$$v_L = \frac{Q^4}{q^4} \tag{2}$$

$$v_T = \tan^2\frac{\theta}{2} - \frac{Q^2}{2q^2}, \tag{3}$$

where θ is the scattering angle.

In the impulse approximation the electron is assumed to scatter off individual nucleons inside the nucleus through the one-body current, inducing one-particle–one-hole (1p1h) excitations in the nuclear system. The response functions are then

$$R_K(q,\omega) = \frac{V}{(2\pi)^3}\int d^3h \frac{(m_N^*)^2}{E_p E_h} 2w_K(\mathbf{p},\mathbf{h}) \times \delta(\omega + E_h - E_p)\theta(p - k_F)\theta(k_F - h) \tag{4}$$

where $K = L, T$, and $\mathbf{p} = \mathbf{h} + \mathbf{q}$ by momentum conservation. The functions $w_K(\mathbf{p},\mathbf{h})$ are the responses for the 1p1h excitation. With the z-axis aligned along the momentum transfer $\mathbf{q}$ they are

$$w_L = w^{00}, \qquad w_T = w^{xx} + w^{yy} \tag{5}$$

where $w^{\mu\nu}$ is the single-nucleon hadronic tensor

$$w^{\mu\nu}(\mathbf{p},\mathbf{h}) = \frac{1}{2}\sum_{s_p s_h} j^\mu(\mathbf{p},\mathbf{h})^* j^\nu(\mathbf{p},\mathbf{h}), \tag{6}$$

and j^μ is the electromagnetic current of the nucleon

$$j^\mu(\mathbf{p},\mathbf{h}) = \bar{u}_{s_p}(\mathbf{p})\left[F_1(Q^2)\gamma^\mu + F_2(Q^2)\frac{i\sigma^{\mu\nu}Q_\nu}{2m_N}\right]u_{s_h}(\mathbf{h}), \tag{7}$$

where u_s are Dirac spinors with mass m_N^*. The RMF response described above corresponds to either protons or neutrons separately; the total nuclear response is then obtained by summing the proton and neutron contributions. Note that the vector potential energy, E_v, cancels out in the energy difference between the particle and hole states, Eq. (4), so the nuclear response does not depend on it.

One of the key assumptions of scaling approaches is the factorization of the nuclear response into a averaged single-nucleon response and a function that encapsulates the nuclear dynamics. In the RFG model, this factorization is exact, as can be readily seen in the following way. We first integrate over the angular variables in Eq. (4), using the energy-conserving delta function, and arrive at

$$R_K(q,\omega) = \frac{V}{(2\pi)^3}\frac{2\pi m_N^{*3}}{q}\int_{\epsilon_0}^{\epsilon_F} n(\epsilon) 2w_K(\epsilon,q,\omega). \tag{8}$$

Here $\epsilon = E_h/m_N^*$ is the hole energy in units of the effective nucleon mass, $\epsilon_F = E_F/m_N^*$ refers to the Fermi energy in the same units, and $n(\epsilon) = \theta(\epsilon_F - \epsilon)$. The lower limit ϵ_0 is given by (see Appendix C of [43] for a detailed derivation)

$$\epsilon_0 = \mathrm{Max}\left\{\kappa\sqrt{1 + \frac{1}{\tau}} - \lambda, \epsilon_F - 2\lambda\right\}. \tag{9}$$

Here we are using dimensionless variables

$$\kappa = \frac{q}{2m_N^*}, \qquad \lambda = \frac{\omega}{2m_N^*}, \qquad \tau = \kappa^2 - \lambda^2. \tag{10}$$

Now we can define an average value of the single-nucleon response as follows:

$$\bar{w}_K(q,\omega) = \frac{\int_{\epsilon_0}^{\epsilon_F} n(\epsilon) w_K(\epsilon, q, \omega)}{\int_{\epsilon_0}^{\epsilon_F} n(\epsilon)}, \tag{11}$$

allowing us to express the total response in a factorized form:

$$R_K(q,\omega) = \frac{V}{(2\pi)^3} \frac{2\pi m_N^{*3}}{q} 2\bar{w}_K(q,\omega) \int_{\epsilon_0}^{\infty} n(\epsilon). \tag{12}$$

This expression can be further transformed by:

(i) assuming that the nuclear volume V is related to the number of nucleons $\mathcal{N}$ through the Fermi momentum k_F as $\frac{V}{(2\pi)^3} = \frac{\mathcal{N}}{\frac{8}{3}\pi k_F^3}$,

(ii) defining the scaling function $f(\psi)$ as

$$\frac{3}{4} \int_{\epsilon_0}^{\infty} n(\epsilon) d\epsilon \equiv (\epsilon_F - 1) f^*(\psi^*), \tag{13}$$

(iii) and defining the scaling variable as

$$\psi^* = \sqrt{\frac{\epsilon_0 - 1}{\epsilon_F - 1}} \mathrm{sgn}(\lambda - \tau). \tag{14}$$

The sign convention is chosen so that ψ^* is negative when $\lambda < \tau$ (to the left of the quasielastic peak), equals zero at the peak ($\lambda = \tau$), and is positive when $\lambda > \tau$ (to the right of the peak).

Note that with these definitions, the scaling function takes the simple parabolic form

$$f^*(\psi^*) = \frac{3}{4}(1 - \psi^{*2})\theta(1 - \psi^{*2}). \tag{15}$$

With this, the nuclear response function can be written as

$$R_K(q,\omega) = \bar{w}_K(q,\omega) \mathcal{N} \frac{2}{q} \left(\frac{m_N^*}{k_F}\right)^3 (\epsilon_F - 1) f^*(\psi^*). \tag{16}$$

This expression can be transformed into the simplified form

$$R_K(q,\omega) = r_K(q,\omega) f^*(\psi^*), \tag{17}$$

by introducing the so-called single-nucleon prefactors r_K,

$$r_K(q,\omega) = \bar{w}_K(q,\omega) \mathcal{N} \frac{2}{q} \left(\frac{m_N^*}{k_F}\right)^3 (\epsilon_F - 1), \tag{18}$$

which contain not only the averaged nucleon responses but also other kinematic and normalization factors that, strictly speaking, belong to the full nuclear response. Nevertheless, the term "single-nucleon factors" has become standard in the literature. In any case, the total response is obtained by combining the proton and neutron contributions

$$R_K(q,\omega) = (Zr_K^p + Nr_K^n) f^*(\psi^*), \tag{19}$$

where the prefactors r_K^p (r_K^n) contain the averaged response of the proton (neutron), $\bar{w}_K^p$ ($\bar{w}_K^n$). When the nuclear response is divided by the total prefactor $(Zr_K^p + Nr_K^n)$, what remains is the superscaling function $f^*(\psi^*)$, which is independent of the momentum transfer q and of the nuclear species when expressed as a function of the scaling variable ψ^*. This variable has been constructed such that its range always lies within the interval $[-1, 1]$.

In the SuSAM approach, the selected quasielastic (e, e') cross section data are divided by the corresponding combination of longitudinal and transverse single-nucleon prefactors, including the appropriate kinematic factors and the Mott cross section. This defines the phenomenological superscaling function $f^*(\psi^*)$,

$$f^*_{\mathrm{exp}}(\psi^*) = \frac{\left(\frac{d\sigma}{d\Omega d\omega}\right)_{\mathrm{exp}}}{\sigma_{\mathrm{Mott}}[v_L(Zr_L^p + Nr_L^n) + v_T(Zr_T^p + Nr_T^n)]}. \tag{20}$$

Among the data scaled using the procedure described above, a careful selection was carried out to isolate genuine quasielastic events. This was achieved by excluding data points that exhibited large deviations from the scaling trend, typically associated with inelastic excitations or very low energy transfers, where scaling violations are more prominent. This selection strategy was systematically applied in a series of works, initially focused on ^{12}C, and later extended to a global fit encompassing nuclei from deuterium up to uranium [33,34]. The result was a remarkably good overall description of inclusive quasielastic electron scattering cross sections across the nuclear chart using a small number of parameters and a single phenomenological scaling function. This function was parametrized through a sum of Gaussians to capture its shape accurately. The model was subsequently applied to neutrino scattering data [44], where the inclusion of 2p2h excitations proved essential [39,41]. In further developments, the model was refined to account for the high-ψ^* tail of the scaling function. This tail was interpreted as arising from processes involving the emission of two nucleons, potentially reflecting the underlying dynamics of short-range correlated nucleon pairs [40].

III. DEVELOPMENT OF SUSAM-V2

Despite the overall success of scaling models based on a single phenomenological scaling function in describing quasielastic lepton-nucleus scattering, the SuSAM-v1 framework presents some limitations. In particular, it does not accurately reproduce the separated longitudinal (R_L) and transverse (R_T) nuclear response functions. The use of an effective nucleon mass within SuSAM-v1 allows for a successful description of the inclusive cross section, but only as some average of R_L and R_T, rather than capturing each component correctly. This limitation becomes especially relevant in the context of neutrino scattering, where the different nuclear response functions contribute with distinct weights. Moreover, the transverse channel is significantly enhanced by the presence of axial-vector currents, which contribute in addition to the purely vector responses present in electron scattering. There also appears a new interference response, $R_{T'}$, arising from the coupling between vector and axial currents. In this section, we construct the SuSAM-v2 model as an improved approach aimed at addressing these shortcomings by enabling a more accurate and consistent description of the separated response functions.

A key step in refining the SuSAM-v2 model is the introduction of two independent scaling functions, f_L and f_T, corresponding to the longitudinal and transverse nuclear responses, respectively. This extension is motivated by the observation that the longitudinal response function, R_L, approximately exhibits superscaling behavior, making it suitable for the direct extraction of f_L from experimental data. In contrast, the transverse response R_T does not scale as well due to the influence of additional reaction mechanisms, such as meson-exchange currents and inelastic contributions, and therefore cannot be used straightforwardly to extract f_T. Instead, f_T will be determined phenomenologically by fitting inclusive quasielastic cross section data, following a procedure similar to that used in the original SuSAM-v1 approach, as will be detailed later.

(i) *Longitudinal scaling function* We begin by analyzing the experimental data for the longitudinal scaling function, which is obtained from R_L by dividing out the appropriate single-nucleon prefactor

$$f_L^*(\psi^*)_{\exp} = \frac{R_L^{\exp}}{Zr_{Lp} + Nr_{Ln}}. \tag{21}$$

In Fig. 1 we show the values of the longitudinal scaling function $f_L^*(\psi^*)$ obtained from experimental data of R_L for ^{12}C, scaled according to the procedure described above. The figure illustrates that the longitudinal response exhibits approximate scaling behavior when plotted as a function of ψ^*. Although the scaling is not perfect, the deviations remain within the experimental uncertainties, making it feasible to fit a longitudinal scaling function $f_L^*(\psi^*)$ to all the data points. Given the observed asymmetry in the shape of the distribution, a sum of two Gaussian functions provides a suitable phenomenological fit:

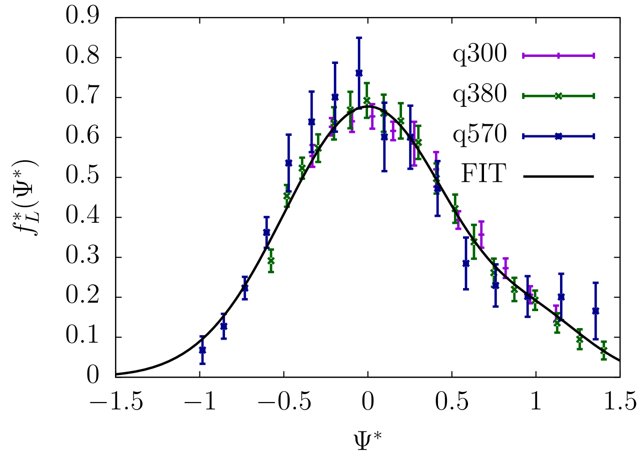

FIG. 1. Phenomenological longitudinal scaling function used in this work. Data are for three values of $q = 300, 380, 570$ MeV/c from Refs. [3,45].

$$f_L^*(\psi^*) = a_1 e^{-\frac{(\psi^*-b_1)^2}{2c_1^2}} + a_2 e^{-\frac{(\psi^*-b_2)^2}{2c_2^2}}. \tag{22}$$

The parameters a_i (center), b_i (width), and c_i (height) obtained for this model are presented in Table I.

It is worth noting that the present longitudinal scaling function $f_L^*(\psi^*)$ differs from the function $f_L(\psi)$ previously extracted in Ref. [46], which did not incorporate the effective mass. In contrast, the new function $f_L^*(\psi^*)$ still benefits from the dynamical relativistic effects associated with the RMF model, as these are embedded through the use of the effective mass in the scaling variable and the single-nucleon prefactors.

(ii). *Transverse scaling function* We now proceed to determine the new transverse scaling function $f_T^*(\psi^*)$ by fitting quasielastic cross section data for ^{12}C after subtracting the longitudinal contribution. This longitudinal part is computed using the phenomenological scaling function $f_L^*(\psi^*)$ extracted in the previous step. We begin with inclusive electron scattering data in the quasielastic region and, as a first step, subtract the contribution from MEC in the two-particle emission channel. This contribution is evaluated using a microscopic model within the RMF framework [41,42]. In the second step, we subtract the

TABLE I. Parameters for the phenomenological longitudinal scaling function described by the sum of two Gaussians.

Parameter	Value
a_1	0.67732
b_1	0.0
c_1	0.497381
a_2	0.103387
b_2	1.05065
c_2	0.302541

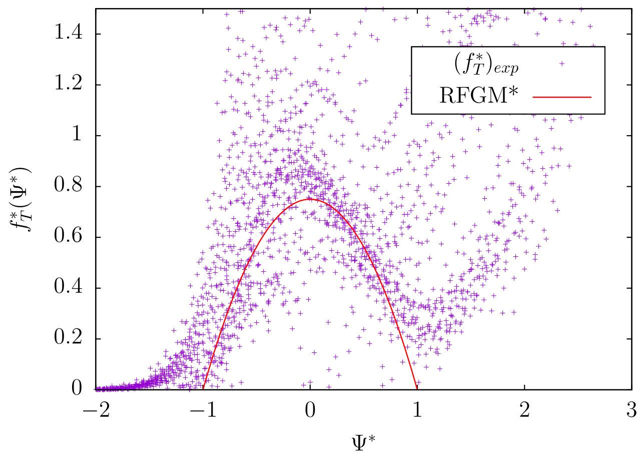

FIG. 2. Transverse scaling function data obtained from the cross section data after using Eqs. (23) and (24), compared with the Fermi gas model scaling function using an effective mass $M^* = 0.8$.

longitudinal contribution already fixed by $f_L^*(\psi^*)$. The remaining strength is assumed to be entirely transverse in nature:

$$(R_T)_{\rm exp} = \frac{(\frac{d\sigma}{d\Omega d\omega})_{\rm exp} - (\frac{d\sigma}{d\Omega d\omega})_{2p2h} - \sigma_M v_L R_L}{\sigma_M v_T}. \quad (23)$$

Dividing $(R_T)_{\rm exp}$ by the single-nucleon transverse response gives the experimental transverse scaling function data:

$$(f_T^*)_{exp} = \frac{(R_T)_{\rm exp}}{Z r_T^p + N r_T^n}. \quad (24)$$

Applying this procedure to the experimental (e, e') cross section data for ^{12}C—consisting of approximately 3000 data points available from the University of Virginia database [47,48]—and representing the results as a function of the scaling variable ψ^*, we obtain the distribution shown in Fig. 2. It is apparent from the figure that the scaled data still include significant contributions from inelastic nucleon excitations, such as pion production and deep inelastic scattering. The next step in the analysis is to remove these inelastic contributions by means of a subtraction procedure.

A careful analysis of the behavior of the experimental data as a function of the transferred momentum q indicates that the quasielastic scaling function must carry an additional dependence on q, similar to what was already implemented in the SuSA-v2 approach. This momentum dependence cannot be ignored if one aims to accurately reproduce the structure of the data across the full kinematic range. To account for this, we performed independent fits by dividing the data into 18 intervals of q, as detailed in Table II. A subset of 15 of these intervals is displayed in separate panels in Fig. 3, where we show the scaled experimental cross section data grouped according to

TABLE II. Parameters of the transverse scaling function fitted by a Gaussian with three parameters a, b, and c for different momentum transfer intervals.

q_i	q_f	a	b	c
0	230	0.20	0.58	0.24
230	240	0.25	0.55	0.30
240	270	0.52	0.30	0.38
270	290	0.55	0.25	0.38
290	320	0.53	0.25	0.58
320	340	0.70	0.14	0.45
340	360	0.70	0.20	0.45
360	380	0.76	0.10	0.48
380	410	0.76	0.07	0.45
410	460	0.83	0.02	0.45
460	500	0.84	0.01	0.45
500	550	0.83	0.01	0.45
550	610	0.84	−0.01	0.46
610	680	0.82	−0.07	0.46
680	760	0.83	−0.09	0.46
760	820	0.80	−0.11	0.48
820	1000	0.80	−0.15	0.48
1000	5000	0.83	−0.25	0.45

increasing q, from $q < 230$ MeV/c to $q > 1000$ MeV/c. The exact boundaries of all intervals are provided in the table.

To extract the transverse scaling function in each momentum transfer region, we fit the scaled cross section data using a sum of three phenomenological Gaussian functions. The first Gaussian corresponds to the quasielastic peak, the second describes the contribution from the $\Delta(1232)$ resonance, and the third accounts for the rise observed at higher energies due to deep inelastic scattering (DIS). For momentum transfers below $q < 300$ MeV$/c$, the third Gaussian is omitted from the fit, as the experimental data show no significant contribution from inelastic processes in this regime. It is important to emphasize that this procedure does not rely on a specific microscopic model for pion production or DIS; rather, the region-by-region fitting allows us to determine the best phenomenological parameters that describe each contribution based on the data themselves. If more detailed models for the inelastic channels become available, the fitting strategy could be refined accordingly. However, such fine-tuning is beyond the scope of the present approach, whose main objective is to capture the dominant features of the quasielastic transverse response in a phenomenological and model-independent manner.

The results of the region-by-region fits are also shown in Fig. 3. Data corresponding to very-high-momentum transfers ($q > 1000$ MeV/c), where deep inelastic contributions dominate, are fitted over a wide range of momentum transfers $(1000 < q < 5000)$ MeV$/c$. Additionally, for some low-q intervals ($q < 360$ MeV$/c$) and low energy, certain data points that clearly do not exhibit scaling

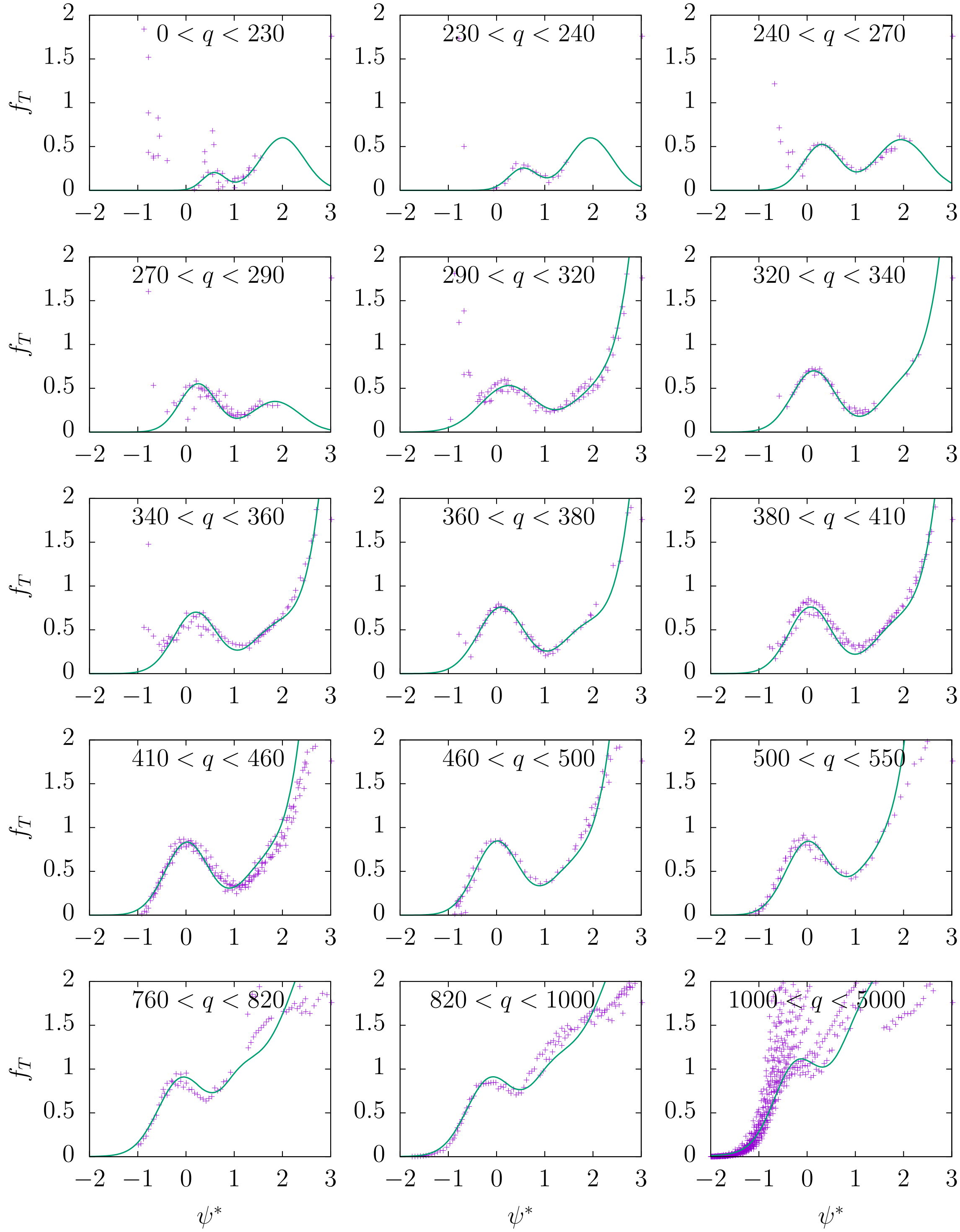

FIG. 3. Experimental transverse scaling function datasets corresponding to different intervals of the momentum transfer. The green line represents a fit using two or three Gaussian functions.

behavior were not taken into account for the fit. This selection was performed by visually inspecting each momentum bin and discarding points that deviate significantly from the quasielastic scaling trend. After this data selection and fitting procedure, the first Gaussian in each momentum transfer interval is identified as the phenomenological transverse scaling function, defined independently for each q-bin:

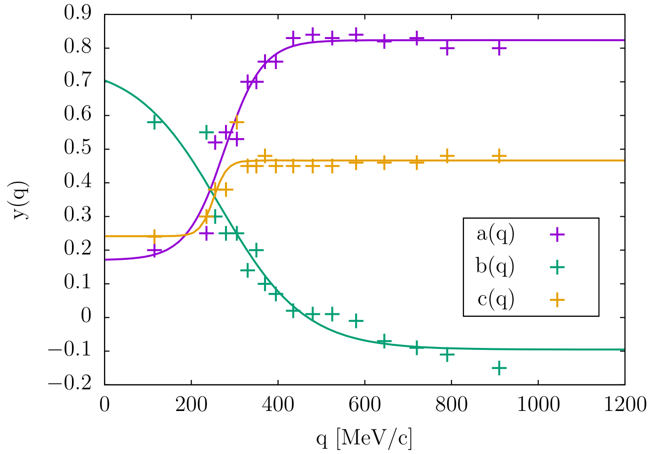

FIG. 4. Coefficients $a(q)$, $b(q)$, and $c(q)$ of the transverse scaling function as a function of the momentum transfer, fitted using a Fermi function.

$$f_T^*(\psi^*, q) = a(q) e^{-\frac{(\psi^* - b(q))^2}{2c(q)^2}}. \tag{25}$$

The parameters of the transverse scaling function f_T, denoted as $a(q)$, $b(q)$, and $c(q)$, are listed in Table II for each momentum transfer interval. These parameters exhibit a clear dependence on q. In particular, the position of the peak, given by $b(q)$, shows a noticeable shift: it starts around $b \sim 0.5$ for low-q values (below 240 MeV/c), then decreases rapidly, crossing zero near $q = 500$ MeV/c, and becomes increasingly negative, reaching approximately $b = -0.25$ at $q = 1000$ MeV/c. Similarly, the height of the scaling function, $a(q)$, increases with q up to around 400 MeV/c, where it stabilizes. The width parameter $c(q)$ follows a similar trend, stabilizing for $q \gtrsim 300$ MeV/c. This explicit momentum-transfer dependence is essential to accurately reproduce the behavior of the cross section in the low-q region, where violations of scaling are more pronounced. Therefore, the inclusion of this q-dependence in the updated SuSAM-v2 model is expected to significantly improve the description of the quasielastic region at low-momentum transfers, which could not be adequately captured using a scaling function independent of q.

This behavior of the parameters is more clearly illustrated in Fig. 4, where they are plotted as a function of the momentum transfer q. It is found that this dependence can be accurately described using a single Fermi function for each parameter,

$$y(q) = \frac{\alpha_1}{1 + e^{(q-\alpha_2)/\alpha_3}} + \alpha_4, \tag{26}$$

where $y = a, b, c$. This provides a smooth parametrization of the transverse scaling function $f_T^*(\psi^*, q)$. The corresponding fitted values are listed in Table III. The use of Fermi functions ensures a reliable extrapolation of the scaling function across a wide range of momentum transfers.

TABLE III. Parameters of the Fermi function that fit the coefficients a, b, and c of the phenomenological transverse scaling function.

Coefficient	$a(q)$	$b(q)$	$c(q)$
α_1	−0.653271	0.851301	−0.224921
α_2 [MeV/c]	276.616	266.775	251.325
α_3 [MeV/c]	44.0707	97.4585	15.5872
α_4	0.823775	−0.0952112	0.466494

The q-dependence observed in the extracted transverse scaling function f_T^* may be, at least in part, attributed to final state interactions (FSI). These effects are known to induce violations of scaling, particularly at low- and high-momentum transfer, due to mechanisms such as nucleon rescattering and absorption [49,50]. Although FSI are not explicitly included in the present model, their effects are effectively incorporated through the phenomenological q-dependence of the scaling function.

IV. RESULTS

Once the new scaling analysis SuSAM-v2 of the electron scattering data has been completed, and the two phenomenological scaling functions $f_L^*(\psi^*)$ and $f_T^*(\psi^*, q)$ have been determined, we proceed to analyze how the model describes the available data for response functions and inclusive cross sections. This includes both electron scattering and predictions for neutrino-induced reactions. The main objective is to assess whether the SuSAM-v2 model provides an improved description compared to the previous SuSAM-v1 version. A positive outcome would reinforce the reliability of the new approach and have important implications for the modeling of quasielastic lepton-nucleus interactions, particularly in the context of neutrino oscillation experiments.

A. Electron scattering

The SuSAM-v2 model preserves the same factorized structure used in the previous version, where the response functions are expressed as the product of a single-nucleon term and a phenomenological scaling function. The most significant difference now is that the longitudinal and transverse responses are computed separately using their respective phenomenological scaling functions, $f_L^*(\psi^*)$ and $f_T^*(\psi^*, q)$, obtained from the independent analysis of longitudinal and transverse electron scattering data. This separation allows for a more flexible and accurate description of each response channel:

$$R_L(q, \omega) = (Z r_L^p + N r_L^n) f_L^*(\psi^*), \tag{27}$$

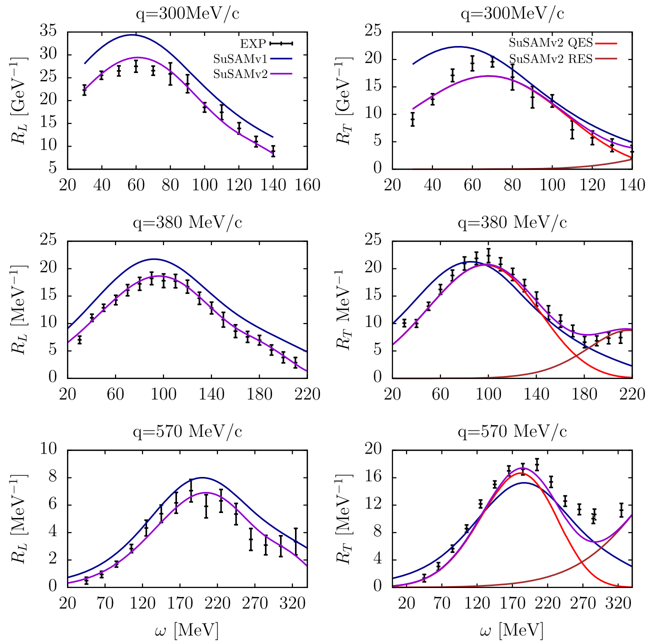

FIG. 5. Separated longitudinal and transverse electromagnetic responses for three momentum transfers: $q = 300$, 380, and 570 MeV$/c$, using the SuSAM-v1 and SuSAM-v2 prescriptions. The results are compared with experimental data from Refs. [3,45].

$$R_T(q,\omega) = (Zr_T^p + Nr_T^n)f_T^*(\psi^*, q). \tag{28}$$

The quasielastic longitudinal and transverse response functions for inclusive (e, e') scattering from ^{12}C are shown in Fig. 5. Alongside the experimental data, we present the theoretical results obtained with the updated SuSAM-v2 model and compare them with those from the previous SuSAM-v1 version. For the transverse response, we also include the contribution from the resonant component that we have subtracted (parametrized as a sum of Gaussians), that contributes to the tail of the T-response for high ω.

The first observation is that the longitudinal response R_L is well reproduced by the SuSAM-v2 model for all three momentum transfers shown. This result is expected, since the R_L data were used directly in the extraction of the scaling function f_L^*. In contrast, the SuSAM-v1 model clearly overestimates R_L, highlighting an initial improvement introduced by the new version. A significant improvement is also observed in the description of the transverse response R_T with SuSAM-v2. This constitutes a genuine prediction of the model, since R_T data were not used in the fit of the transverse scaling function f_T^*—only the inclusive cross section data were employed. This outcome indicates that a simultaneous fit to R_L and to the inclusive cross section, within our analysis framework, leads naturally to a reliable description of R_T. In particular, for $q = 570$ MeV/c, the new model incorporates the necessary enhancement around the quasielastic peak to reproduce the observed data, which was underestimated in the previous version. It is worth highlighting the improved agreement achieved at low-momentum transfer, where scaling violations are more pronounced and the previous model fails to reproduce both the shape and magnitude of the response.

In Fig. 6 we show the inclusive electron scattering cross section on ^{12}C for nine different kinematics, covering low- (top panels), intermediate- (middle panels), and high- (bottom panels) momentum transfers. The results obtained with the updated SuSAM-v2 model are compared with those of the previous version, SuSAM-v1, and with experimental data.

The comparison shows that the SuSAM-v1 model tends to overestimate the cross section at low-momentum transfers, particularly around the quasielastic peak. At higher values of q, it often underestimates the peak height and, in some cases, fails to reproduce the correct peak position. In contrast, the new SuSAM-v2 model exhibits a clear improvement in all these aspects, yielding a more accurate description of both the magnitude and the location of the quasielastic peak across all kinematic regimes.

A noticeable enhancement is also observed at low-energy transfer, especially at low-momentum transfer, where the new model better reproduces the behavior of the data. However, it is worth noting that the description of the region corresponding to giant resonances remains poor, as these data were not included in the fitting procedure and lie outside the quasielastic domain targeted by our model.

Regarding the 2p2h contribution, taken from Refs. [41,42], it is based in a microscopic calculation of meson-exchange currents in the RMF of nuclear matter and an estimation of 2p2h emission by the one-body current describing the high-energy tail of the scaling function. In the figure the 2p2h contribution allows the estimation of its order of magnitude and its potential role in improving the description of the dip region between the quasielastic peak and the onset of pion production. Since our model is designed specifically to describe the quasielastic region, pion production mechanisms are not included. Nonetheless, the inclusion of 2p2h provides a reasonable approximation of the expected enhancement in this transition region.

B. Neutrino scattering

We now proceed to the results section for neutrino-induced reactions. In the case of the (ν_μ, μ^-) process, the double-differential cross section is given by

$$\frac{d\sigma}{dT_\mu d\cos\theta_\mu} = \sigma_0(v_{CC}R_{CC} + 2v_{CL}R_{CL} + v_{LL}R_{LL} + v_TR_T \pm 2v_{T'}R_{T'}), \tag{29}$$

where θ_μ and T_μ are muon scattering angle and kinetic energy, respectively. Here σ_0 is the analogue of the Mott

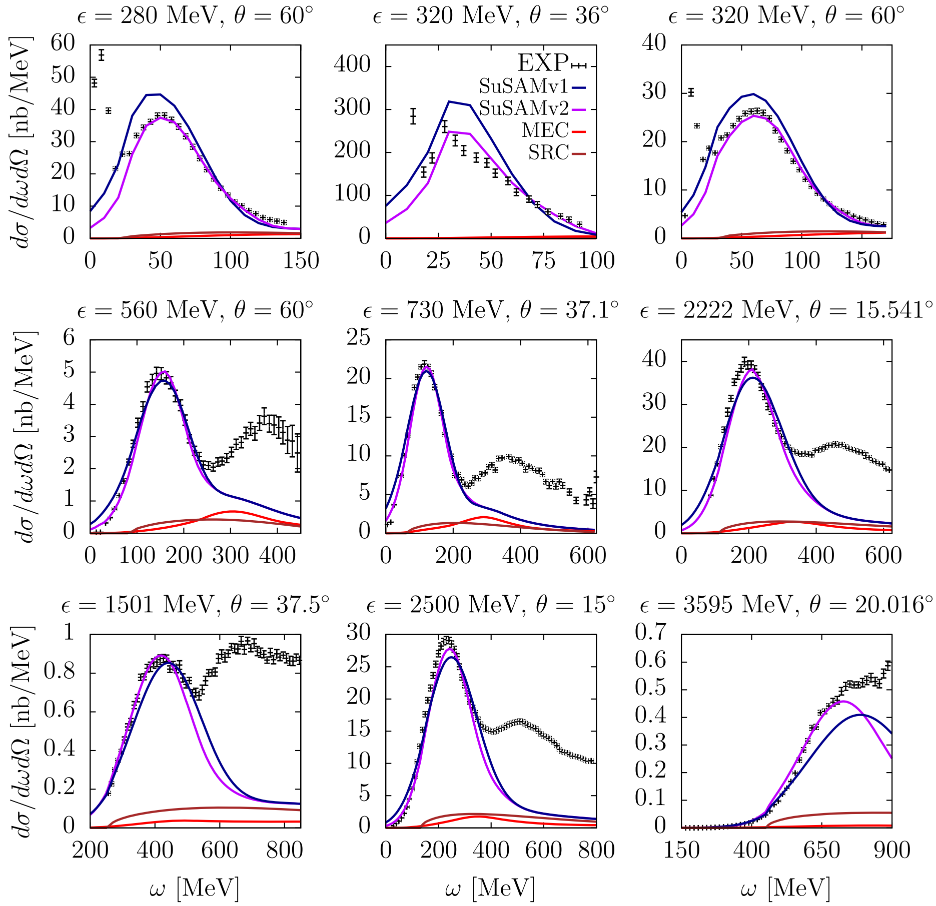

FIG. 6. Inclusive electron scattering cross section on ^{12}C for nine different kinematics. Comparison between low- (top panels), intermediate- (middle panels), and high- (bottom panels) momentum transfer using the SuSAM-v1 and SuSAM-v2 models, including the 2p2h contribution from MEC and an estimation from SRC. The experimental data are taken from Refs. [2,47,48].

cross section for neutrino scattering, the coefficients v_K are purely kinematical factors, and five nuclear response functions $R_K(q,\omega)$ contribute to the cross section (the $\pm$ sign corresponds to neutrino or antineutrino scattering). Detailed definitions of these quantities can be found in Ref. [44].

The SuSAM model assumes that each nuclear response can be factorized into a single-nucleon prefactor multiplied by a universal scaling function. In the original SuSAM-v1 approach, this scaling function was extracted from inclusive electron scattering data and was assumed to be the same for all channels. In the present work, within the SuSAM-v2 framework, we retain the same factorization scheme but distinguish between longitudinal and transverse scaling functions, denoted $f_L^*(\psi^*)$ and $f_T^*(\psi^*,q)$, respectively. Specifically, we write:

$$R_K(q,\omega) = N r_K f_L^*(\psi^*), \qquad K = CC, CL, LL,$$
$$R_K(q,\omega) = N r_K f_T^*(\psi^*,q), \qquad K = T, T',$$

where r_K are the single-nucleon prefactors. In this approach, it is further assumed that the same transverse scaling function applies to both the T and T' channels, i.e., f_T^* is used for both R_T and $R_{T'}$.

One essential difference in neutrino experiments is that the measured cross sections are flux-averaged, meaning they are weighted integrals over the incoming neutrino energy spectrum. Since each experiment has a different neutrino flux, the measured observables effectively emphasize different energy regions of the cross section. This must be taken into account when comparing theory and experiment. The flux-averaged double-differential cross section is computed as

$$\frac{d^2\sigma}{dT_\mu d\cos\theta_\mu} = \frac{\int dE_\nu \Phi(E_\nu) \frac{d^2\sigma}{dT_\mu d\cos\theta_\mu}(E_\nu)}{\int dE_\nu \Phi(E_\nu)}, \qquad (30)$$

where $\Phi(E_\nu)$ is the neutrino flux and $\frac{d^2\sigma}{dT_\mu d\cos\theta_\mu}(E_\nu)$ is the cross section for fixed neutrino energy E_ν.

In this section, we present results for two representative experiments: T2K, which uses a ^{12}C target, and MINERνA (Main Injector Neutrino ExpeRiment to study v-A interactions), which uses a hydrocarbon (CH) target. In each

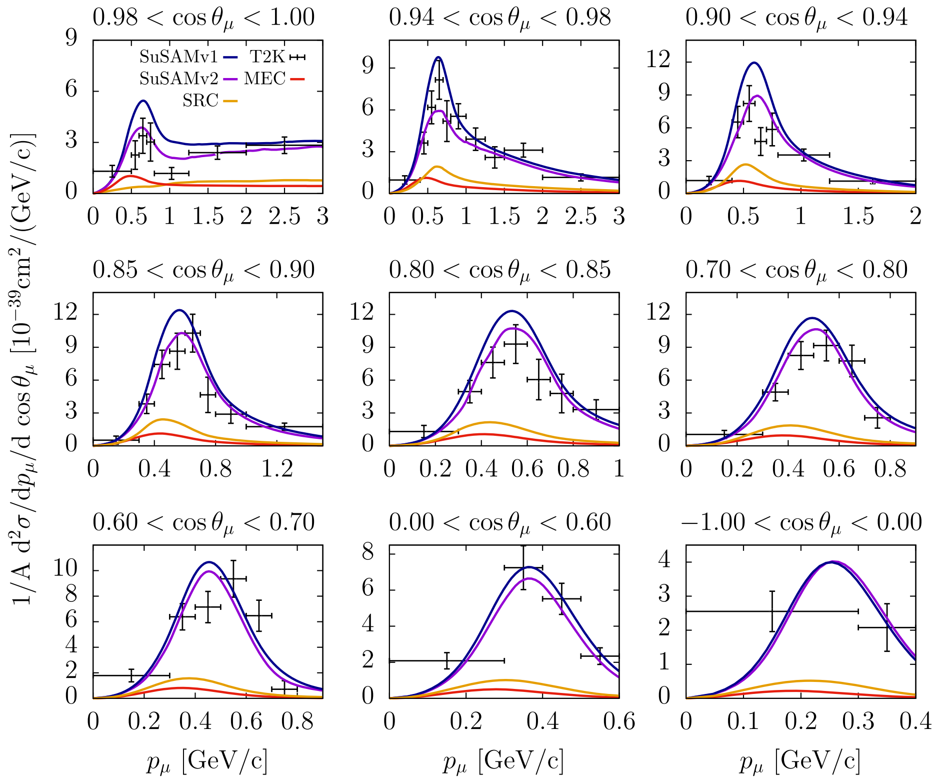

FIG. 7. Neutrino charged-current quasielastic cross section from the T2K experiment, shown as a flux-folded double-differential distribution per nucleon. The comparison has been performed using the SuSAM-v1 and SuSAM-v2 models, including the 2p2h contribution. The experimental data, taken on a ^{12}C target, are from Ref. [53].

case, we compare the predictions of the SuSAM-v1 and SuSAM-v2 models, showing the effects of the updated scaling functions. A model for the 2p2h contribution is also included additively, as it represents an independent reaction channel not captured by the quasielastic scaling functions.

The 2p2h channel includes two separate contributions. The first arises from meson-exchange currents, for which we employ a fully microscopic model as described in Ref. [41] for the inclusive case and in Refs. [51,52] for the semi-inclusive cross section. In this approach, the 2p2h-MEC response functions are calculated using the complete Δ-propagator, with in-medium effects incorporated through an effective mass and a vector energy for the Δ resonance. The calculation is performed under the universal coupling approximation.

The second 2p2h contribution is related to the one-body current and is linked to the emission of correlated nucleon pairs. This term is described using a semiempirical formula introduced in Refs. [40,41], which is proportional to the 2p2h phase space and the nucleon form factors, with fitted coefficients designed to reproduce the high-energy tail of the experimental scaling function. This contribution is phenomenological in nature and is intended as a placeholder for the effects of nucleon-nucleon correlations, in the absence of a complete microscopic model.

We begin by presenting results for the T2K experiment in Fig. 7. The quasielastic cross section is reported in bins of the outgoing muon angle $\cos\theta_\mu$, which are not equally spaced. As a result, an average over each bin width is required to compute the theoretical prediction. Each panel of Fig. 7 displays the cross section as a function of the muon momentum for a given angular bin, comparing the SuSAM-v1 and SuSAM-v2 predictions. The total prediction includes the 2p2h contributions from both MEC and SRC, and we also show these components separately for reference.

The analysis of Fig. 7 reveals that the SuSAM-v2 results are generally reduced compared to those of SuSAM*v1, leading to an improved agreement with the experimental measurements. This improvement is especially significant at small muon scattering angles, where the v1 version tended to overestimate the cross section near the peak. The reduction in SuSAM-v2 arises primarily from two modifications. First, the longitudinal scaling function has been fitted, resulting in a slight decrease of the longitudinal response. Second, the transverse scaling function now depends explicitly on the momentum transfer q; for low q, its height and width are significantly reduced, and its peak position is shifted. These changes contribute to a more accurate description of the cross section at small angles, where low-momentum transfers dominate the response, thus enhancing the overall consistency with the T2K data. The effects of MEC and SRC show similar features, with some variations at very small angles. Both responses peak at lower energies compared to the 1p1h response. The inclusion of 2p2h contributions from both MEC and correlations is important for accurately describing the data, accounting for roughly 20% of the total cross section.

To conclude this work, we compare the model predictions with the double-differential cross sections measured by the MINERνA experiment on a CH target. The MINERνA data provide a stringent test for theoretical models, as they span a wide kinematic range with neutrino energies extending well beyond 1.5 GeV and cover longitudinal muon momenta up to 20 GeV. This implies that the corresponding momentum transfers probe regions significantly higher than those accessed in lower-energy experiments such as T2K, which is largely limited to momentum transfers below 1 GeV/c. The cross sections are reported as functions of the muon momentum components parallel and perpendicular to the incoming neutrino direction, variables which are particularly sensitive to nuclear effects and allow for a more differential analysis of the reaction dynamics. An important feature of MINERνA is its ability to isolate the quasielastic-like contribution from other channels, enabling a focused comparison with theoretical predictions in the QE region. Moreover, these data provide valuable insight into the role of multinucleon emission mechanisms: our analysis includes both meson-exchange currents and short-range correlation contributions in the 2p2h sector, which turn out to be essential for a consistent description of the measured cross sections.

Figure 8 presents the comparison between the SuSAM model predictions and the double-differential cross sections measured by MINERνA as functions of the transverse muon momentum p_T for fixed bins of longitudinal momentum $p_\parallel$ ranging from 1.5 GeV to 8 GeV. The predictions from both SuSAM-v1 and the updated SuSAM-v2 models are shown. In all cases, the theoretical cross sections include both the quasielastic contribution and the 2p2h components. As observed in the figure, both versions of the model provide a very good description of the experimental data across the full kinematic range. The agreement holds for low- and high-$p_\parallel$ bins, with both SuSAM-v1 and SuSAM-v2 reproducing the shape and magnitude of the cross sections. The overall differences between the two versions are small. The most noticeable difference appears in the width of the distribution as a function of p_T: the SuSAM-v2 prediction is slightly narrower, especially in the lower $p_\parallel$ bins. This reflects the impact of the updated scaling functions $f_L^*(\psi^*)$ and $f_T^*(\psi^*, q)$ introduced in SuSAM-v2, which were extracted

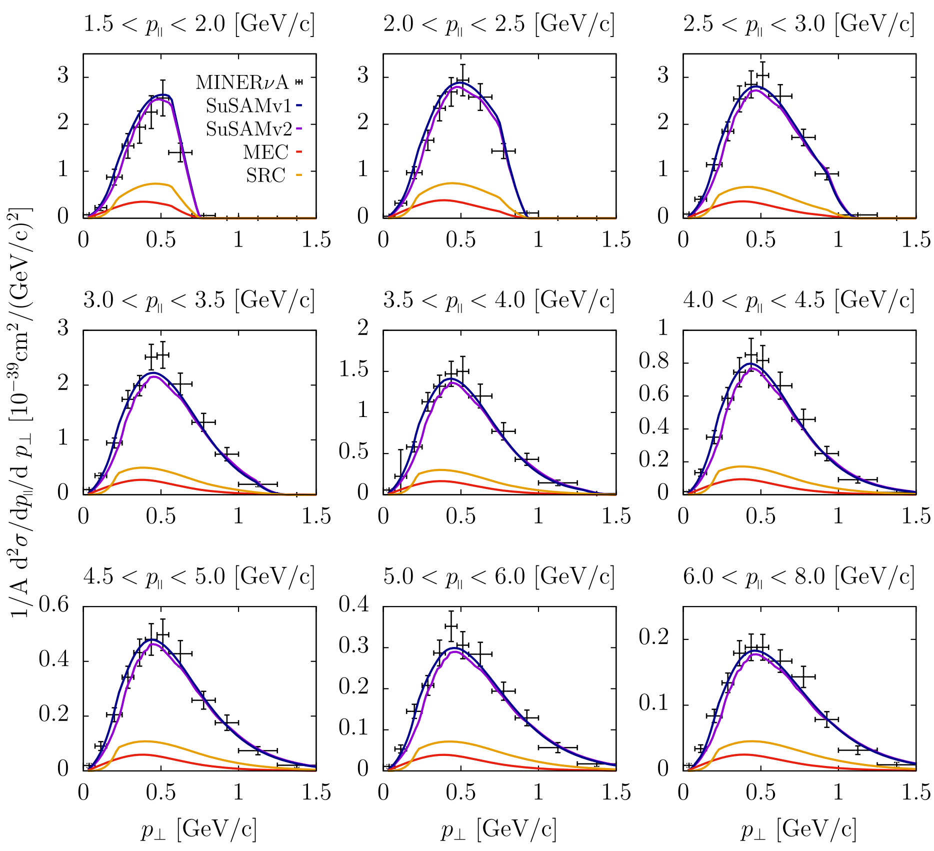

FIG. 8. Neutrino charged-current cross section from the MINERνA experiment, shown in bins of transverse muon momentum and as a function of parallel muon momentum. The comparison has been performed using the SuSAM-v1 and SuSAM-v2 models, including the 2p2h contribution. The experimental data, taken on CH target, are from Ref. [54].

independently from longitudinal and transverse electron scattering data, respectively.

The similarity between the two models in this particular dataset can be attributed to the neutrino flux of MINERνA, which peaks at relatively high energies. At large momentum transfers, where both models yield similar scaling behavior and the longitudinal and transverse responses converge, the differences between SuSAM-v1 and SuSAM-v2 become less significant.

Another important feature of the comparison is the size of the 2p2h contribution. In all kinematic bins, the inclusion of the 2p2h response—driven by MEC and SRC—leads to a visible enhancement of the total cross section. The contribution of 2p2h processes is non-negligible, amounting to approximately 30% of the total cross section in most bins. This confirms the relevance of multinucleon effects in the interpretation of inclusive neutrino-nucleus data and underlines the need for their consistent incorporation in theoretical models, especially for oscillation experiments.

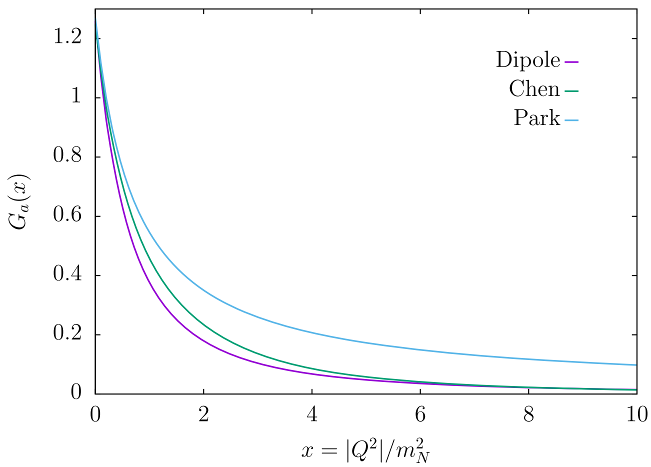

FIG. 9. Axial form factor of the nucleon as a function of $x = |Q^2|/m_N^2$, comparing the traditional dipole form with recent parametrizations from [55–57].

While SuSAM-v1 already provided a satisfactory description of the MINERνA data, the updated SuSAM-v2 model reinforces these results by offering a more flexible and accurate framework. The independent treatment of the longitudinal and transverse nuclear responses improves the predictive power of the model, particularly at lower energies and in situations where the separation of response functions becomes essential. Although the differences between v1 and v2 are minor in the case of MINERνA, SuSAM-v2 is expected to provide significant improvements in other kinematical regions and for other observables where SuSAM-v1 is less reliable.

The axial form factor of the nucleon is commonly modeled using the standard dipole parametrization with $G_A(0) = 1.26$ and an axial mass $M_A = 1.032$ GeV. This choice ensures consistency with previous SuSAM-based analyses. However, recent experimental and lattice QCD studies [55–57] indicate noticeable deviations from the dipole shape, particularly at intermediate momentum transfers, as shown in Fig. 9. These findings suggest that more refined descriptions of G_A may be needed to reduce systematic uncertainties in neutrino-nucleus scattering models. A full analysis of these effects is beyond the scope of the present work; nevertheless, to illustrate their potential impact, in Fig. 10 we compare the

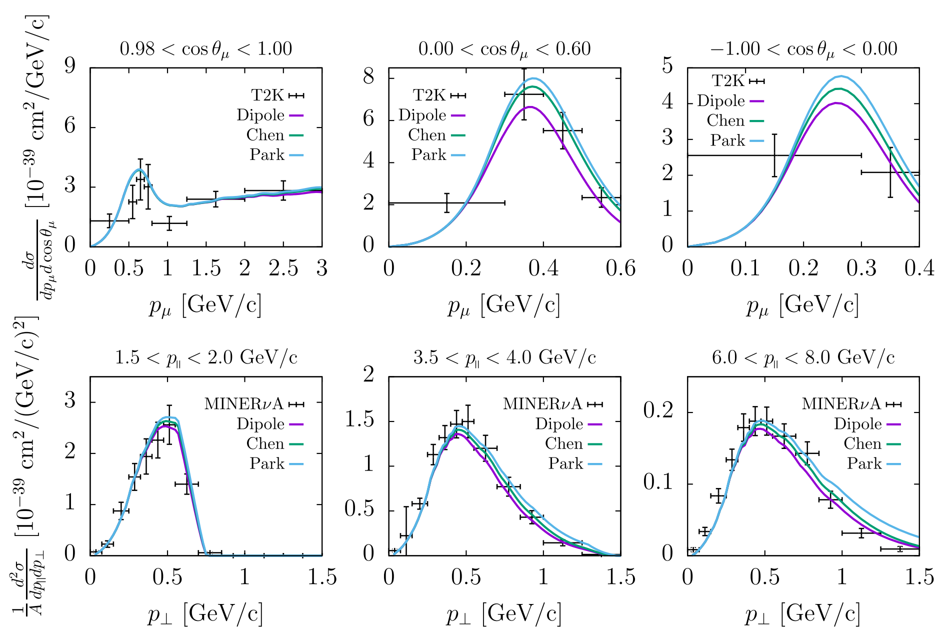

FIG. 10. Impact of different axial form factor parametrizations on the predicted cross sections. The calculations use dipole (standard), Chen *et al.* [55,56], and Prat *et al.* [57] parametrizations for selected T2K and MINERvA kinematics.

double-differential cross sections obtained using different axial form factor parametrizations (namely, those of Dipole, Chen, and Park) for selected kinematic configurations relevant to T2K and MINERνA. The results show that the differences between parametrizations can reach nonnegligible levels in specific regions of phase space, in some cases increasing the predicted cross section by up to 25% at the QE-peak. This emphasizes the importance of a more accurate treatment of the axial structure in precision neutrino physics.

V. CONCLUSIONS

In this work, we have developed and tested a new version of the SuSAM model—SuSAM-v2—for describing quasielastic lepton-nucleus scattering. The model is based on the scaling analysis of inclusive electron scattering data, which allows the nuclear responses to be factorized into a single-nucleon cross section and a universal scaling function. The key improvement introduced in SuSAM-v2 is the separate treatment of the longitudinal and transverse scaling functions, $f_L^*(\psi^*)$ and $f_T^*(\psi^*, q)$, both extracted from electron scattering data and fitted independently. These functions are parametrized with simple analytical forms, enabling an efficient and transparent implementation of the model across a wide kinematic range. The transverse scaling function in SuSAM-v2 is extracted independently for each momentum transfer interval using a model-independent procedure, where the contributions from pion production and deep inelastic scattering are subtracted. The resonance region is not described in detail but rather approximated in a coarse manner, with the sole purpose of identifying and isolating the quasielastic domain; the rest of the inelastic spectrum is disregarded in the scaling analysis.

Compared to the earlier SuSAM-v1, which employed a common scaling function for all nuclear responses, SuSAM-v2 provides an improved description of the separated longitudinal and transverse electromagnetic response functions, particularly at intermediate- and low-momentum transfers. This enhancement translates directly into a more accurate and flexible framework for predicting neutrino-nucleus cross sections in the quasielastic channel. We have validated the model by comparing its predictions with $^{12}\mathrm{C}(e, e')$ cross sections, and T2K and MINERνA data for CC muon neutrino scattering, showing excellent agreement in both shape and magnitude of the double-differential cross sections, including the contributions from 2p2h excitations, computed with a semiempirical model.

All superscaling models—including SuSAM—are ultimately phenomenological parametrizations of the inclusive cross section, each incorporating different nuclear ingredients. In the case of SuSAM, the effective mass of the nucleon in the medium plays a central role in shaping the scaling variable and the nuclear dynamics. This contrasts with the widely used SuSA model, which does not include an effective mass but requires the use of an empirical separation energy to shift the scaling function. Despite these differences, both models reproduce inclusive electron and neutrino scattering data with comparable accuracy.

Notably, both SuSAM-v2 and SuSA-v2 incorporate a transverse scaling function that depends on the momentum transfer q. However, while SuSA-v2 derives this function from an RMF model for finite nuclei—resulting in a numerically defined, nonanalytic function—SuSAM-v2 provides an explicit analytical parametrization based on a Gaussian form, whose parameters vary smoothly with q. This feature makes SuSAM-v2 particularly well suited for use in Monte Carlo event generators and phenomenological studies, where reproducibility and computational efficiency are essential. Scaling-based parametrizations such as SuSAM-v2 provide a valuable alternative to fully microscopic approaches, offering both physical transparency and practical advantages for interpreting experimental data and supporting neutrino oscillation analyses. Multiple models based on scaling approaches offers the possibility to estimate the theoretical or model-dependent systematic uncertainties that affect neutrino cross section analyses and oscillation experiments. As neutrino experiments continue to improve in precision, phenomenological models with solid empirical foundations and simple implementations will remain a key tool in understanding the complex dynamics of neutrino-nucleus interactions.

ACKNOWLEDGMENTS

We thank Jesus Gonzalez-Rosa and Jorge Segovia for helpful discussions. V. L. M. C. acknowledges financial support provided by Ministerio Español de Ciencia, Innovación y Universidades under Grant No. PID2022-140440NB-C22; Junta de Andalucía under Contracts No. PAIDI FQM-370 and No. PCI+D+i under the title: “Tecnologías avanzadas para la exploración del universo y sus componentes” (Code AST22-0001). The work was supported by Grant No. PID2023-147072NB-I00 funded by MICIU/AEI/10.13039/501100011033 and by ERDF/EU, and also by Grant No. FQM-225 funded by Junta de Andalucia.

DATA AVAILABILITY

The data are not publicly available. The data are available from the authors upon reasonable request.

[1] T. W. Donnelly and I. Sick, Rev. Mod. Phys. **56**, 461 (1984).
[2] O. Benhar, D. Day, and I. Sick, Rev. Mod. Phys. **80**, 189 (2008).
[3] J. Jourdan, Nucl. Phys. **A603**, 117 (1996).
[4] J. A. Formaggio and G. P. Zeller, Rev. Mod. Phys. **84**, 1307 (2012).
[5] L. Alvarez-Ruso *et al.*, Prog. Part. Nucl. Phys. **100**, 1 (2018).
[6] R. A. Smith and E. J. Moniz, Nucl. Phys. **B43**, 605 (1972).
[7] J. M. Udías, J. A. Caballero, E. Moya de Guerra, J. E. Amaro, and T. W. Donnelly, Phys. Rev. Lett. **83**, 5451 (1999).
[8] J. A. Caballero, J. E. Amaro, M. B. Barbaro, T. W. Donnelly, C. Maieron, and J. M. Udias, Phys. Rev. Lett. **95**, 252502 (2005).
[9] R. González-Jiménez, M. B. Barbaro, J. A. Caballero, T. W. Donnelly, N. Jachowicz, G. D. Megias, K. Niewczas, A. Nikolakopoulos, and J. M. Udías, Phys. Rev. C **101**, 015503 (2020).
[10] A. Meucci, C. Giusti, and F. D. Pacati, Phys. Rev. C **83**, 064614 (2011).
[11] J. Nieves, I. Ruiz Simo, and M. J. Vicente Vacas, Phys. Rev. C **83**, 045501 (2011).
[12] V. Pandey, N. Jachowicz, T. Van Cuyck, J. Ryckebusch, and M. Martini, Phys. Rev. C **92**, 024606 (2015).
[13] O. Benhar, A. Fabrocini, and S. Fantoni, Nucl. Phys. **A505**, 267 (1989).
[14] J. E. Amaro, M. B. Barbaro, J. A. Caballero, T. W. Donnelly, and A. Molinari, Nucl. Phys. **A723**, 181 (2003).
[15] J. E. Amaro, M. B. Barbaro, J. A. Caballero, T. W. Donnelly, C. Maieron, and J. M. Udias, Phys. Rev. C **81**, 014606 (2010).
[16] T. Franco-Munoz, J. García-Marcos, R. González-Jiménez, and J. M. Udías, Phys. Rev. C **108**, 064608 (2023).
[17] A. Fabrocini, Phys. Rev. C **55**, 338 (1997).
[18] M. Petraki, E. Mavrommatis, O. Benhar, J. W. Clark, A. Fabrocini, and S. Fantoni, Phys. Rev. C **67**, 014605 (2003).
[19] J. Carlson, J. Jourdan, R. Schiavilla, and I. Sick, Phys. Rev. C **65**, 024002 (2002).
[20] J. Carlson, S. Gandolfi, F. Pederiva, S. C. Pieper, R. Schiavilla, K. E. Schmidt, and R. B. Wiringa, Rev. Mod. Phys. **87**, 1067 (2015).
[21] A. Lovato, S. Gandolfi, J. Carlson, S. C. Pieper, and R. Schiavilla, Phys. Rev. Lett. **112**, 182502 (2014).
[22] T. W. Donnelly and I. Sick, Phys. Rev. Lett. **82**, 3212 (1999).
[23] W. M. Alberico, A. Molinari, T. W. Donnelly, E. L. Kronenberg, and J. W. Van Orden, Phys. Rev. C **38**, 1801 (1988).
[24] M. B. Barbaro, R. Cenni, A. De Pace, T. W. Donnelly, and A. Molinari, Nucl. Phys. **A643**, 137 (1998).
[25] D. B. Day, J. S. McCarthy, T. W. Donnelly, and I. Sick, Annu. Rev. Nucl. Part. Sci. **40**, 357 (1990).
[26] C. Maieron, T. W. Donnelly, and I. Sick, Phys. Rev. C **65**, 025502 (2002).
[27] T. W. Donnelly and I. Sick, Phys. Rev. C **60**, 065502 (1999).
[28] A. Bodek and M. E. Christy, Phys. Rev. C **106**, L061305 (2022).
[29] A. Bodek, M. E. Christy, Z. Lin, G. M. Bulugean, and A. M. Delgado, arXiv:2410.15991.
[30] A. Bodek, M. E. Christy, Z. Lin, G. M. Bulugean, A. M. Delgado, A. M. Ankowski, G. D. Megias, and J. Tena Vidal, arXiv:2409.10637.
[31] R. Gonzaléz-Jiménez, G. D. Megias, M. B. Barbaro, J. A. Caballero, and T. W. Donnelly, Phys. Rev. C **90**, 035501 (2014).
[32] J. E. Amaro, M. B. Barbaro, J. A. Caballero, T. W. Donnelly, R. Gonzalez-Jimenez, G. D. Megias, and I. R. Simo, Eur. Phys. J. Special Topics **230**, 4321 (2021).
[33] V. L. Martinez-Consentino, I. Ruiz Simo, J. E. Amaro, and E. Ruiz Arriola, Phys. Rev. C **96**, 064612 (2017).
[34] J. E. Amaro, V. L. Martinez-Consentino, E. Ruiz Arriola, and I. Ruiz Simo, Phys. Rev. C **98**, 024627 (2018).
[35] R. Rosenfelder, Ann. Phys. (N.Y.) **128**, 188 (1980).
[36] K. Wehrberger, Phys. Rep. **225**, 273 (1993).
[37] C. J. Horowitz and B. D. Serot, Nucl. Phys. **A368**, 503 (1981).
[38] B. D. Serot and J. D. Walecka, The relativistic nuclear many-body problem, in *Advances in Nuclear Physics* (Springer, Boston, MA, 1986), pp. 1–327.
[39] V. L. Martinez-Consentino, J. E. Amaro, and I. Ruiz Simo, Phys. Rev. D **104**, 113006 (2021).
[40] V. L. Martinez-Consentino, J. E. Amaro, P. R. Casale, and I. Ruiz Simo, Phys. Rev. D **108**, 013007 (2023).
[41] V. L. Martinez-Consentino and J. E. Amaro, Phys. Rev. D **108**, 113006 (2023).
[42] V. L. Martinez-Consentino, I. R. Simo, and J. E. Amaro, Phys. Rev. C **104**, 025501 (2021).
[43] J. E. Amaro, M. B. Barbaro, J. A. Caballero, R. González-Jiménez, G. D. Megias, and I. R. Simo, J. Phys. G **47**, 124001 (2020).
[44] I. Ruiz Simo, V. L. Martinez-Consentino, J. E. Amaro, and E. Ruiz Arriola, Phys. Rev. D **97**, 116006 (2018).
[45] J. Jourdan, Phys. Lett. B **353**, 189 (1995).
[46] J. E. Amaro, M. B. Barbaro, J. A. Caballero, T. W. Donnelly, A. Molinari, and I. Sick, Phys. Rev. C **71**, 015501 (2005).
[47] O. Benhar, D. Day, and I. Sick, arXiv:nucl-ex/0603032.
[48] O. Benhar, D. Day, and I. Sick, http://faculty.virginia.edu/qes-archive/.
[49] J. Arrington, C. S. Armstrong, T. Averett, O. K. Baker, L. de Bever, C. W. Bochna, W. Boeglin, B. Bray, R. D. Carlini, G. Collins *et al.*, Phys. Rev. Lett. **82**, 2056 (1999).
[50] O. Benhar, Phys. Rev. Lett. **83**, 3130 (1999).
[51] V. L. Martinez-Consentino, A. M. Cantizani, and J. E. Amaro, Phys. Rev. C **109**, 015502 (2024).
[52] V. L. Martinez-Consentino and J. E. Amaro, Symmetry **16**, 247 (2024).
[53] K. Abe *et al.* (T2K Collaboration), Phys. Rev. D **93**, 112012 (2016).
[54] D. Ruterbories *et al.* (MINERvA Collaboration), Phys. Rev. D **99**, 012004 (2019).
[55] C. Chen and C. D. Roberts, Eur. Phys. J. A **58**, 206 (2022).
[56] C. Chen, C. S. Fischer, C. D. Roberts, and J. Segovia, Phys. Lett. B **815**, 136150 (2021).
[57] S. Park *et al.* (Nucleon Matrix Elements (NME) Collaboration), Phys. Rev. D **105**, 054505 (2022).